Industrial-Scale Treatment of Biological Tissues with Pulsed Electric Fields

H. Bluhm and M. Sack

Abstract In this section we discuss the technical requirements and perspectives for industrial-scale electroporation of plant cell tissues. Energetically it seems more favorable to apply strong fields and short pulses than weak fields and long pulses. Different generator configurations for the production of strong pulsed electric fields and the durability of their main components are considered. Schemes for the process control and the verification of the achieved degree of electroporation are examined. In the second part of this contribution we describe the status of some emerging industrial applications like sugar beet treatment, extraction of aromas, and flavors from wine grapes, and the conditioning of green biomass for energetic utilization by electroporation-assisted dewatering.

1 Introduction

The present contribution will be restricted to the industrial exploitation of permanent pores (permeability) induced by strong pulsed electric fields (PEFs) in the membranes of plant cells, a process usually termed electroporation. A detailed description of electroporation has been given in Chapters 1 and 2 of this book and will not be repeated here. Stress reactions enhancing the production of certain substances in the cell interior or influencing the growth of fungi, which also have been reported in the literature (Tsukamoto et al. 2003), will not be considered.

The treatment of plant cell tissues with PEFs as a supplementary step or a substitute for existing procedures in a food processing chain is justified only if economic, ecologic, or qualitative advantages can be realized. These advantages can result from an increased yield of nutriments, shorter process times, reduced energy consumption, or a longer shelf life of the product.

Industrial-scale treatment of plant cell tissues generally demands for large throughputs. A large sugar factory, for example, is capable to process a sugar beet flow rate of up to 600 t/hour, while the capacity of a fruit dejuicing plant is typically

H. Bluhm
Forschungszentrum Karlsruhe GmbH, Institute for Pulsed Power and Microwave Technology, Postfach 3640, D-76021 Karlsruhe
e-mail: bluhm@ihm.fzk.de

E. Vorobiev, N. Lebovka (eds.), *Electrotechnologies for Extraction from Food Plants and Biomaterials*, DOI: 10.1007/978-0-387-79374-0_9,

of the order of 100 t/hour. A large throughput can either be realized by a large flow cross-section or a high flow velocity. Evidently a robust, reliable, and inexpensive technology for the production of adequately strong electric fields in large volumes is a prerequisite for a successful industrial utilization of electroporation. The formation of large irreversible pores is a function of the product of field strength E and pulse duration τ. Energetically it seems more favorable to create the permanent pores with strong fields and short pulses than with weak fields and long pulses. To illustrate this let us consider a flow of sugar beet cossettes with a packing density of 60%. To maintain the integrity of the cossettes the flow velocity needs to be restricted to less than 1.5 m/s. In our example the cross-section of the field zone is assumed to be 0.3×0.3 m^2 and its length 1.50 m. Thus, the sugar beet throughput corresponds to 290 t/hour and the time during which a cell remains in the reactor becomes 1 s. There is a threshold of about 0.5 V for the potential across a membrane that needs to be exceeded before pores begin to grow. Assuming a mean size of 100 μm for the sugar beet cells, we can conclude that a minimum field strength of 10 kV/m is required. For a pulse duration of 1μs, typically 30 pulses with 500 kV/m are necessary to open the membrane. Let us now compare the two extreme cases of DC operation at 10 kV/m with that of pulsed operation at 500 kV/m, 30 Hz repetition rate, and 1μs pulse width. The conductivity of a suspension of sugar beet cossettes is on the order of 0.3 S/m. In case of DC operation we need a voltage amplitude of 3 kV and the ohmic current becomes 1.35 kA. Thus, the high-voltage supply must deliver an average power of 4.05 MW. In case of pulsed operation, a voltage amplitude of 150 kV and a pulsed current of 67.5 kA are needed. However, the average power reduces to 160 kW.

The requirements for pulse generators suitable for industrial-scale treatment of plant cell tissues have been summarized in Table 1.

Besides supplying the requested electrical parameters, the pulse generator should allow a low maintenance rate and a long durability of components to meet the economic requirements.

2 Pulse Generators for Industrial Applications

2.1 Generator Configurations

The parameters summarized in Table 1 can be realized through different generator configurations. The simplest setup is a high-voltage capacitor or a parallel

Table 1 Requirements for industrial-scale pulse generators

Parameter	Value
Pulse amplitude	100 kV–1 MV
Pulse current	10–100 kA
Power of pulse	1–10 GW
Pulse duration	1–10 μs
Average power	100–500 kW
Repetition rate	1–50 Hz
Component lifetime	10^9 pulses

connection of several capacitors discharged into the reaction chamber through a closing switch. A variant of this configuration is the Blumlein setup shown in Fig. 1a. Here two LC chains are charged in parallel and discharged in series thus doubling the output voltage. The main problem with all of these configurations is to achieve the required pulse amplitude of several hundred kilovolts. Of course it is conceivable to increase the output voltage by a pulse transformer as shown in Fig. 1b. However, the core of this transformer needs to be quite large since the core cross section F multiplied with the sum of the saturation inductance B_s and the remnant inductance B_r of the ferromagnetic material must be greater than the time integral of the voltage pulse U(t):

$$F(B_r + B_s) > \int U(t)\mathrm{d}t \tag{1}$$

For a voltage amplitude of 100 kV and a pulse duration of several μs F can reach several tenth of a square meter. Another disadvantage is that the pulse transformer does not only change the voltage amplitude but also multiplies the impedance of the generator with the square of the transformation factor n. For this reason and to avoid pulse deformation, n has to be limited.

Therefore, a more attractive configuration is the Marx generator whose principle is shown in Fig. 1c. The Marx generator consists of several high voltage capacitors that are charged in parallel from a high-voltage power supply and by closing a set of switches discharged in series (Marx 1923, 1924). Using a Marx configuration it is easily possible to achieve megavolts in output voltage.

A generator consisting of a set of LC chains in a Marx generator configuration (Fig. 1d) is capable of delivering a high rectangular shaped output voltage without the use of a transformer. But due to the larger amount of elements such a device is much more complex and costly than a Marx generator. For many industrial applications the higher efficiency of a rectangular pulse compared to a rather slowly rising and exponentially decaying pulse of a Marx generator is not required.

An important parameter of the Marx generator is its impedance Z, which we define as $\sqrt{L/C}$, where L is the total inductance of the circuit including the inductance of the connections between the Marx and the reactor and C is the serial capacitance of the erected Marx generator $C = C_s/k$ (C_s = stage capacitance, k = number of stages) (Bluhm 2006). In general the electroporation reactor can be considered as a purely resistive load R and the actual voltage at the reactor U_{max} is determined by the ratio of the Marx impedance and the load resistance. This ratio also determines the percentage of voltage reversal U_{rev} at the Marx capacitors which is an important parameter for the lifetime of high-voltage capacitors and should not exceed the value rated by the constructor of the capacitor. Typically it should be less than 20% of the maximum rated voltage. The necessary electric fields inside the reactor and the allowable voltage reversal determine the range of acceptable variations of the reactor resistance R resulting from variations in the conductance of the cell suspension flowing through the reactor.

Analyzing the equivalent circuit of the erected Marx generator with a total erected voltage U_0 connected to the load, we obtain the following expressions for the relative amplitude U_{max}/U_0 and for the fractional voltage reversal U_{rev}/U_0 as

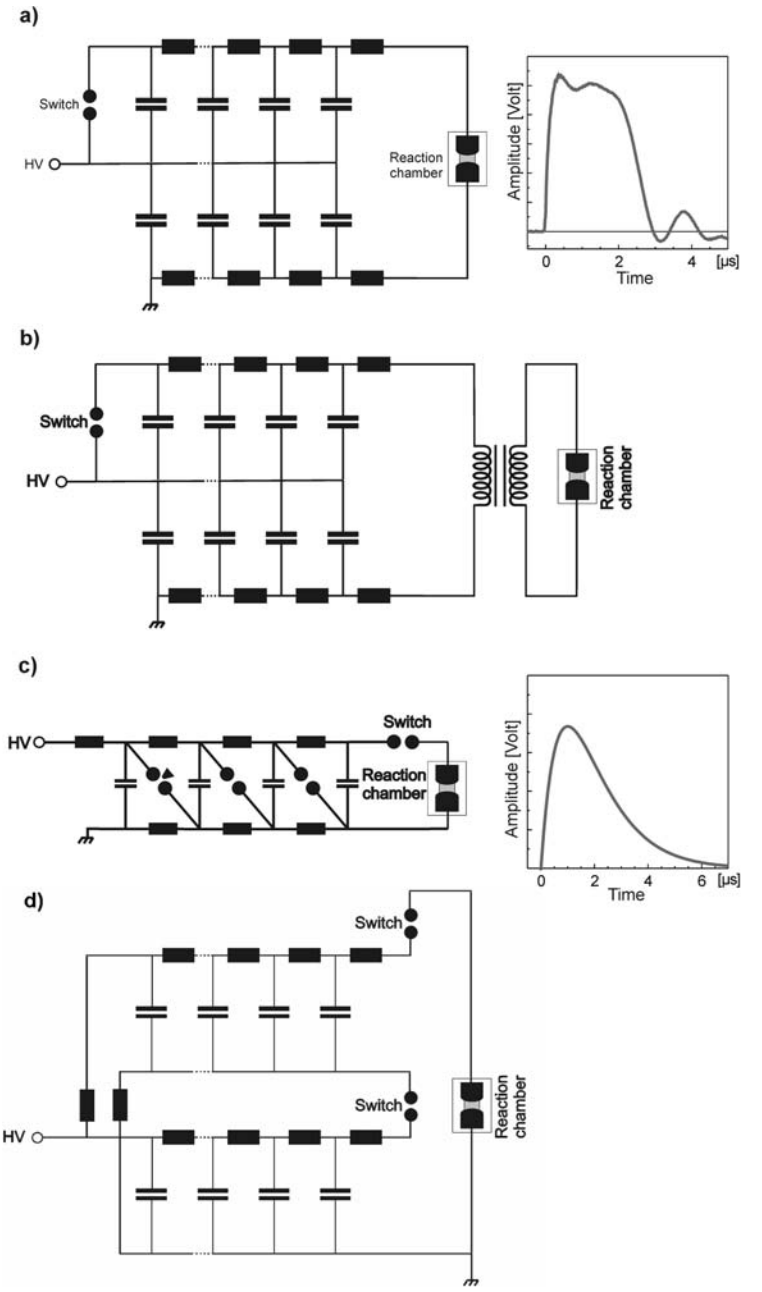

Fig. 1 Possible generator configurations for industrial-scale electroporation. (**a**) and (**b**) LC chains in Blumlein configuration without and with a high voltage pulse transformer. (**c**) Marx generator. (**d**) Two-stage Marx generator with LC chains. The diagrams on the right-hand side show the attainable pulse shapes

a function of the ratio Z/R:

$$\frac{U_{\max}}{U_0} = \frac{1}{\sqrt{\left(\frac{Z}{R}\right)^2 - \frac{1}{4}}} \exp\left(-\frac{\alpha + k\pi}{2\sqrt{\left(\frac{Z}{R}\right)^2 - \frac{1}{4}}}\right) \sin(\alpha + k\pi) \tag{2}$$

$$\frac{U_{\text{rev}}}{U_0} = \exp\left(-\frac{k\pi}{2\sqrt{\left(\frac{Z}{R}\right)^2 - \frac{1}{4}}}\right) \tag{3}$$

where α is given by

$$\alpha = \arctan\left(2\sqrt{\left(\frac{Z}{R}\right)^2 - \frac{1}{4}}\right) \tag{4}$$

The equations above are given for the periodically damped case with $Z > \frac{1}{2} R$ only, as the aperiodically damped case is of less interest for industrial electroporation devices. Equations (2) and (3) have been plotted in Fig. 2. The crosshatched area is the granted operating range for a permitted reversal of up to 30% and an accepted reduction of the pulse amplitude down to 45% of its maximum. Commonly the impedance of a repetitive multistage Marx-generator exceeds 20 Ω while the exemplary reactor described in the introduction represents a resistance between 4 Ω and 8 Ω. Therefore, several Marx generators connected in parallel will be required to drive a large-scale reactor. The problem of synchronizing these generators will be discussed later.

Figure 3 shows two prototype Marx generators that were built to drive a demonstration plant for sugar beet treatment (Schultheiss et al. 2004). They consisted of

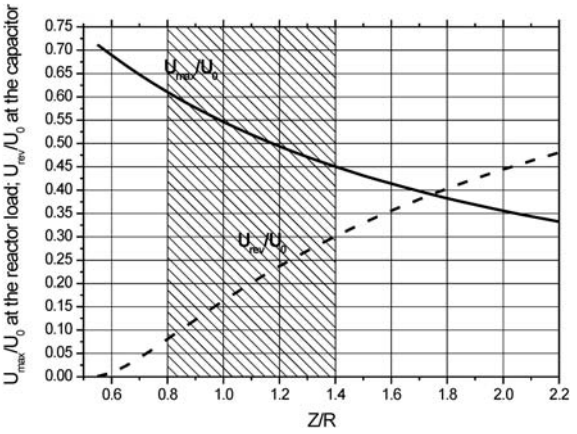

Fig. 2 Voltage amplitude $U_{\max}$ and the voltage reversal U_{rev} of a Marx generator divided by the total erected voltage U_0 as a function of the ratio of the Marx impedance Z and reactor resistance R

Fig. 3 Seven-stage Marx generators built to drive a demonstration plant for sugar beet treatment

seven stages and were able to deliver a voltage pulse with a total erected voltage $U_0 = 350$ kV at a repetition rate of up to 20 Hz. The low energy-density capacitors were rated for a lifetime of more than 10^9 shots.

2.2 Spark Gap Switches

The spark gap switches used in the generators shown in Fig. 3 were contained in a common cylindrical polyethylene tube and operated in a self-break mode. Ignition occurred when the capacitors had been charged past the breakdown voltage of the first switch gap whose interelectrode distance had been reduced compared to the others. Thus, a consecutive ignition of switches was enforced and the breakdown of the following gaps was facilitated through illumination with UV light from the arcs of the preceding ones. Nitrogen gas was circulated through the switch housing both for cooling and removing of the debris that was eliminated from the gas stream by filters.

Also for industrial-scale generators spark gap switches seem more favorable than solid state switches. Gas filled spark gaps are simple, robust, and inexpensive. The

high complexity and the large dimensions of a high-voltage, high-current thyristor stack, for example, which also lead to large product costs, have up to now prevented the broad use of solid state switches in pulsed power applications. The complexity is increased by protective circuits often necessary to prevent the destruction of the device in case of any malfunction in the circuit.

Nevertheless there are also major problems connected with the use of spark gap switches. Their main problem is the burn-up of the switch electrodes. Erosion does not only lead to an enlargement of the interelectrode gap but also to a change—in most cases a roughening—of the electrode surface and to a contamination of the switching gas with dust and gaseous reaction products. The combination of these effects can result in a strong change of the ignition properties and ultimately limits the lifetime of the switch. Also precipitation of debris from the electrodes on the inner wall of the switch housing can contribute to this degradation. Two measures have been taken to retard the alteration of the switching characteristics: profiling of the field distribution on the electrode surface and selection of suitable materials. A uniform field distribution across the electrode surface can provide a homogeneous burn-up. This has been reached by shaping the surface with a Borda profile (Borda 1766).

Figure 4 shows a set of switch electrodes machined with such a profile inside the switch housing. If in addition the surface area of the electrode is made large the growth rate of the interelectrode gap is slowed down. The onset of electrode erosion requires a sufficiently high locally restricted energy deposition that either leads to mechanical stress, local melting or evaporation of the material (Donaldson 1990, 1991). A complete modeling of the electrode burn-up in a spark gap is very complex, and quantitative scaling laws descending from it will probably never become available (Belkin 1971; Belkin and Kiselev 1977). For that aim not only the melting and evaporation of the material have to be calculated but also magnetohydrodynamic and

Fig. 4 Set of spark gap switches with Borda electrode profiles in a common switch housing

acoustic effects expelling the material from the melt zone need to be considered. In addition, the plasma physics in the spark channel and the influence of evaporating material on the plasma properties have to be simulated. On the other hand, if one restricts the simulation to isolated phenomena we can only expect some hints for the selection of suitable electrode materials and for a possible qualitative scaling of the burn-up with current, pulse duration, kind of gas, etc. It turns out that the load integral $\int_0^{t_p} I(t)^2 \mathrm{d}t$ is a useful parameter to describe the phenomena (Zingerman 1960). One can derive the following formula that relates the load integral with the material and spark channel properties:

$$\int_0^{t_p} I(t)^2 \mathrm{d}t = \frac{T_{\mathrm{eff}}^2 \rho\, c' \kappa}{U_c} \cdot \pi^3 b^4 \tag{5}$$

Here I(t) is the current flowing through the spark; t_p is the pulse duration; $T_{\mathrm{eff}} = T_m T_0$ is the difference between the melting point of the electrode material and its initial temperature; ρ is the material density; $c' = c + \Delta H_m / T_{\mathrm{eff}}$ is the reduced specific heat taking into account the melt heat ΔH_m; κ is the heat conductivity; U_c is the cathode fall and b is the arc radius. We can see from Equation (5) that the admissible load integral before the beginning of melting increases with the square of the melting temperature, the product $\rho c' \kappa$, and the spark channel radius b with a power of 4 and it is inversely proportional to the square of the cathode fall ${U_c}^2$. The problem with Equation (5) is that neither the channel radius b nor the cathode fall U_c and their parametric dependence on the nature of the switching gas and the switch current are known.

A similar equation like Equation (5) can be derived for the onset of evaporation. However, for the range of currents and pulse durations of interest here electrode erosion is dominated by the molten volume and not by evaporation.

A different form of Equation (5) can be derived if we introduce the heat flux $\Gamma_0 = U_c I / \pi b^2$ and solve for the melting temperature T_{eff}:

$$T_{\mathrm{eff}} = \frac{\Gamma_0 \sqrt{t_p}}{\sqrt{\rho c' \kappa}\sqrt{\pi}} \tag{6}$$

From the above considerations we can derive the following criteria for the selection of electrode materials: Preferable are materials with large values of $\rho c' T_{\mathrm{eff}}$ and $\sqrt{\bar{\kappa}\, \rho c'} T_{\mathrm{eff}}$. The first parameter describes the necessary specific energy to melt the electrode material while the second is proportional to the heat flux required for the onset of melting. Here $\bar{\kappa}$ is the mean heat conductivity between room temperature and the melting point. A classification of materials based on these parameters is presented in Table 2.

Composite materials try to take advantage of the different physical properties of their components (Haufe et al. 1972; Donaldson 1991). Among these materials CuW is most frequently used for spark gap electrodes. Besides CuW, CuCr and CuCrZr are commonly applied. CuW exploits the good heat conductivity of copper and the

Table 2 Classification of possible electrode materials based on the assumption that melting is the dominating erosion mechanism

Material	T_m[K]	$\bar{\kappa}$[J/s cm K]	c'[J/g K]	$\rho c' T_{eff}$[J/cm^3]	$\sqrt{\rho c' \bar{\kappa}} T_{eff}$ [J/cm^{2}s$^{1/2}$]
Tungsten	3695	1.105	0.271	$1.75 \cdot 10^4$	$7.97 \cdot 10^3$
Molybdenum	2896	1.38	0.251	$6.54 \cdot 10^3$	$4.78 \cdot 10^3$
Copper	1357	3.54	0.727	$6.56 \cdot 10^3$	$4.83 \cdot 10^3$
Niobium	2750	0.537	0.265	$5.45 \cdot 10^3$	$2.65 \cdot 10^3$

high melting point of tungsten. In table 3 the thermophysical properties of Cu, W, and Cr have been listet. CuW consists of a spongy matrix of tungsten that has been impregnated with copper. Since the melting temperature of Cu is much below that of W, molten Cu remains with a certain probability within the solid tungsten matrix. If the heat transfer between copper and tungsten occurs sufficiently fast copper begins to evaporate before tungsten starts to melt because even the evaporation temperature of copper is lower than the melting point of tungsten. On the other hand the heat of evaporation of copper is more thanthree times larger than the heat of melting of tungsten. Therefore, it is expected that the heat flux to the electrode for material erosion can be appreciably larger than for pure copper or tungsten. The mixing ratio for minimum erosion depends also on the structure of the matrix. According to experimental experience the lowest erosion rates appear at 30–40% of Cu.

Important for the success of the matrix concept is the rapidity of temperature equilibration between the components. In this respect the heat conductivity of the material component with the lower boiling temperature, the heat transfer coefficient between components, and the structure of the matrix are crucial parameters.

At required current levels above 10 kA, it seems impossible to eliminate the burn-up of electrodes. Therefore, the self-breakdown level of spark gaps will change during operation and needs to be compensated periodically. This can either be achieved by reducing the gas pressure or by mechanically readjusting the gap width.

Some experience with the burn-up of CuW electrodes has been gained in our laboratory (Sack and Bluhm 2005). At a current level of $\hat{I} = 4.5$ kA, pulse width of $t_h = 1.4$ μs, and load integral of 20 A^{2}s averaging over 500 000 pulses, the mean material losses were found to be 183 ng per pulse for one pair of electrodes. At the working level of an industrial Marx generator of $t =$ 9.5 kA, $t_h = 1.15$ μs pulse width, and a load integral of 82 A^{2}s, losses of 824 ng per pulse have been measured.

Table 3 Thermophysical properties of Cu, W, and Cr to explain the properties of composite materials. $\bar{c}$, $\bar{\kappa}$ are the mean heat capacitance and thermal conductivity respectively

Material	T_m[K]	T_v[K]	$\bar{\kappa}_m$[J/s K]	$\rho c T_{eff}$ (melting) [J/cm^3]	$\rho c T_{eff}$ (boiling) [J/cm^3]	$\sqrt{\rho \bar{c} \bar{\kappa}} T_{eff}$ (melting) [J/cm^{2}s$^{1/2}$]	$\sqrt{\rho \bar{c} \bar{\kappa}}\ T_{eff}$ (boiling) [J/cm^{2}s$^{1/2}$]
Wolfram	3695	5828	0.95	$1.75 \cdot 10^4$	$1.01 \cdot 10^5$	$7.97 \cdot 10^3$	$2.23 \cdot 10^4$
Kupfer	1357	2835	2.67	$6.56 \cdot 10^3$	$5.61 \cdot 10^4$	$4.83 \cdot 10^3$	$1.93 \cdot 10^4$
Chrom	2180	2944					
Zirkon	2128	4682					

The applied electrodes were machined with a Borda profile of 40 mm diameter. If a maintenance period of 200 million pulses, corresponding to approximately 3 month operation of a generator running at 20 Hz, were acceptable, an increase of the gap distance by 1.9 mm for $\hat{I} = 4.5$ kA and 8.7 mm for $\hat{I} = 9.5$ kA would have been to be compensated, corresponding to about 16% and 73% respectively of the initial gap width of 12 mm. These values demonstrate the severity of electrode wear and request for a permanent and automatic adjustment of the switch self-breakdown level. Since the homogeneous field distribution of the Borda profile fosters the uniform burn-up across the electrode surface, it is possible to reduce the increase of the gap width by enlarging the electrode area. Nevertheless at least for the higher current it seems not feasible to compensate the burn-up just by reducing the gas pressure. Systems for adjusting the gap distance mechanically during operation have therefore been designed. A conceivable control scheme will be discussed later.

2.3 Synchronization

It has been mentioned already that the impedance of a multistage repetitive Marx generator is generally much larger than the equivalent resistance of a large-volume industrial electroporation reactor. Designing the Marx generator to match the reactor impedance, although in principle conceivable, severely enhances the switch electrode burn-up. Therefore it is preferable to divide the total required pulse current between several Marx generators. However, this requires synchronizing their pulse generation. Synchronization can be achieved by triggering the first switch in the Marx generators with a sufficiently low jitter. Triggering of spark gap breakdown is generally obtained with an auxiliary electrode (Bluhm 2006). The partial gap between this electrode and one of the main electrodes is rapidly overvolted with the help of an additional trigger pulse generator. After breakdown of this partial gap, the entire charging voltage appears across the second partial gap and leads to its rapid ignition. The disadvantage of this kind of triggering is the even quicker wear of the exposed trigger electrode. A trigatron-type trigger circuit exhibits as well an increased wear for the same reasons. Therefore, we have developed a new durable trigger concept that does not need a third electrode (Sack et al. 2003, 2005). The principle is shown in Fig. 5.

It is based on the superposition of a voltage pulse on the charging voltage of the first capacitor C_1, which appears across the two-electrode spark gap S_1. For that purpose the ground-side charging coil is replaced by a pulse transformer $T_{1,G}$ connected to an auxiliary pulse generator. The pulse transformer superimposes a voltage pulse to the charging voltage of the stage capacitor. The spark gap S_1 ignites because of overvoltage and launches an ignition wave through the other switches. Additionally, the transformer decouples the auxiliary trigger pulse generator from the load voltage of the Marx capacitors.

In the auxiliary trigger pulse generator, a semiconductor switch connects an energy storage capacitor to the primary of the pulse transformer. Depending on the design the trigger pulse can either be generated when the semiconductor switch

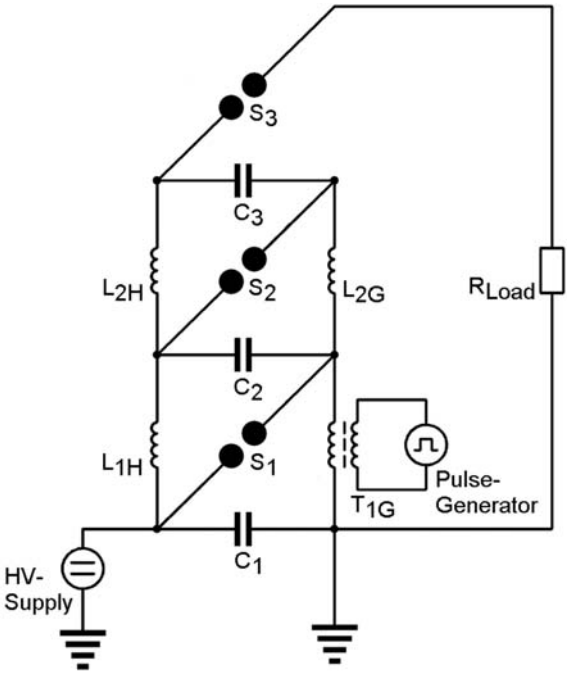

Fig. 5 General scheme of a trigger concept without a trigger electrode based on the superposition of a trigger pulse on the charging voltage of capacitor C_1, which appears across the spark gap S_1

closes or when it subsequently opens. After triggering, the trigger pulse polarity is opposite to the stage voltage across the transformer. Hence, a transient insulation of the two adjacent stages has to be provided by a sufficiently large inductance in the pulse transformer branch. In case of pulse generation at closing time the stages may be insulated either by an increased stray inductance of the pulse transformer, or by an additional series inductance. If the trigger pulse is generated by switch opening, the inductance of the transformer's secondary serves as the transient insulation.

Moreover, the trigger pulse generator has to withstand the voltage appearing across the secondary. Although a closed switch is inherently protected against overvoltage, it has to cope with the current through the charging branch ramping up during pulse formation of the Marx generator. The current driven through the secondary of the transformer flows in the same direction as the current of the trigger pulse. Hence, the switch has to be designed for the sum of both currents. An anti-parallel diode may protect the switch in case of ringing.

An open switch has to be protected against the voltage induced across the primary. The main protective measure is to choose a sufficiently large transformer ratio, which guarantees that the induced voltage remains safely below the maximum voltage rating of the semiconductor switch. Additionally, suppressor diodes may protect the switch. A diode in series to the switch protects it against polarity reversal due to ringing, as for many IGBTs (insulated gate bipolar transistor) or MOSFETs

(metal oxide semiconductor field effect transistor) the reverse breakdown voltage is much less than the forward breakdown voltage.

To obtain a low jitter a fast-rising overvoltage pulse across the spark gap is essential. The stray capacitances of the first stage together with the equivalent inductance of the two charging branches form a resonant circuit determining the rise time of the trigger pulse. If one trigger transformer is implemented e.g. in the ground side charging branch, its effective inductance $L_{\mathrm{T1G,eff}}$ forms together with the charging coil $L_{1\mathrm{H}}$ in the high-voltage side charging branch an inductive voltage divider. The voltage across the spark gap can be calculated from Equation (7) as the sum of the charging voltage of $C_1$and the secondary pulse voltage multiplied by the divider ratio.

$$U_{S_1} = U_{C_1} + \frac{L_{1H}}{L_{1H} + L_{T_{1G},\mathrm{eff}}} U'_{\mathrm{Pulse}} \tag{7}$$

For the fast rising trigger pulse, the stage capacitors C_1 and C_2 can be regarded to be of low impedance. The equivalent inductance of the arrangement is given by

$$L_{1,\mathrm{equ.}} = \frac{L_{1H} \cdot L_{T_{1G},\mathrm{eff}}}{L_{1H} + L_{T_{1G},\mathrm{eff}}} \tag{8}$$

Provided, that both inductances are of the same order the voltage across the spark gap is only approximately half of the secondary trigger pulse amplitude. The equivalent inductance is approximately half of the inductance in each branch.

To compensate for the effect of the voltage divider, the secondary pulse voltage might be increased. But this measure is at the expense of greater effort for the insulation of the pulse transformer, and of more energy required to charge its stray capacitances to a higher voltage. Alternatively, each of the two charging branches can be equipped with the described combination of trigger transformer and trigger pulse generator as shown in Fig. 6. Both pulse generators need to be synchronized since they drive the load in a parallel configuration. If both trigger pulse generators have equal amplitudes, there is no leakage current through either of the two branches.

Using the Marx generator in a common unipolar configuration the pulse circuit consisting of the generator and the electroporation reactor as a load is preferably grounded at the electroporation reactor rather than at the Marx generator. In this way the inductive voltage drop across the ground connection between the generator and the reactor does not lead to any additional current flow along the product stream. Such a leakage current would be undesirable since it reduces the efficiency of the device. But in such a configuration the ground side of the Marx generator floats at 10–20 kV above ground. In case of an accidental flash-over bridging the electrodes inside the electroporation reactor, the floating voltage above ground could become even higher. If the trigger circuitry is empowered from the ground side, the trigger transformers or an extra insulated power supply have to be designed to withstand this voltage. For the transformer–pulse generator combination at the high-voltage side of the charging branch the charging voltage has to be considered additionally.

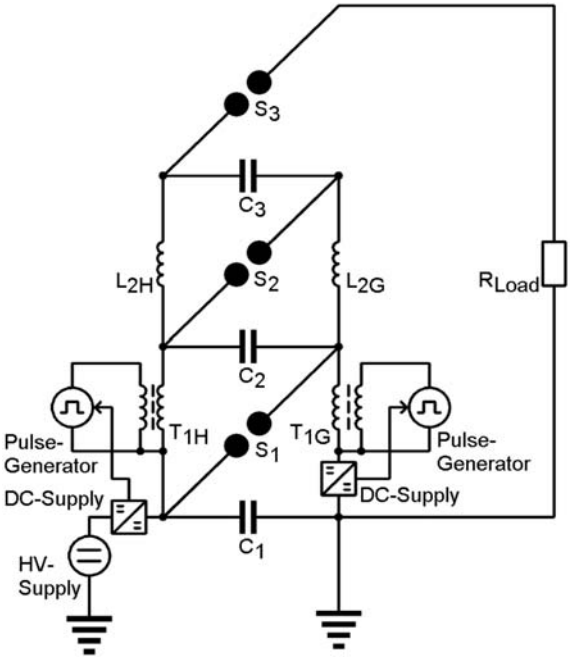

Fig. 6 Improved scheme of a trigger concept without a trigger electrode with one transformer–pulse generator combination in each charging branch powered by the Marx generator's charging current

To overcome these insulation requirements, the trigger pulse generators can be empowered by the charging current of the Marx generator. A DC power supply performs a kind of impedance matching, so that the storage capacitor of the trigger pulse generator can be charged together with the stage capacitors of the Marx generator. Additionally, it delivers the auxiliary power required for the control circuitry and for the fiber-optic receiver used to synchronize the pulse generation.

2.4 Burn-Up Control Scheme

Several possibilities exist to determine the growth of the gap in the switches due to burn-up: Mechanical or optical measurements of the gap width, although possible in principle, are costly and may require periodic interruptions of operation. Therefore, we prefer to derive a control parameter from changes of the switching characteristics itself.

During pulsed breakdown of a spark gap we can distinguish several time steps: t_0 the time until the static breakdown voltage U_0 is exceeded, t_s the statistical delay time until an avalanche effective electron appears in the gap, t_a the avalanche buildup time until the critical charge density for streamer propagation is reached and t_{arc} the time until a low-resistance arc across the gap has been established (Bluhm 2006). If

we assume that the times t_0, t_s, and t_{arc} are short compared to the avalanche buildup time the time integral of the applied voltage U(t) above U_0 is a constant that just depends on the gap geometry (Kind 1958):

$$\int_{t_0+t_s}^{t_0+t_s+t_a} [U(t) - U_0]\,\mathrm{d}t = F \tag{9}$$

Here F is a constant depending on the gap geometry. t_0 and t_s can be considered to be small if the voltage across the gap rises very fast and t_{arc} is always quite short. In addition we can reduce t_s even further if the start electrons are supplied from a corona discharge that appears in the gap during charging of the capacitors. In the trigger scheme described before the shape U(t) of the trigger pulse remains constant. Therefore, any deviations of the integral in Equation (9) reflect changes of the gap geometry which determines both t_a and U_0.

For practical reasons it is advantageous to choose as the control parameter the avalanche buildup time t_a. For that purpose the light pulse from the first spark gap of the Marx generator can be analyzed. If we determine the time difference between the initiation of the trigger generator and the light signal from the spark gap and subtract the constant delay of the trigger circuitry we get a measure of the gap geometry, which can be used to control the gap distance or the switch gas pressure. As the measurement exhibits some scattering due to the jitter, it is necessary to do an averaging before the processing.

Figure 7 demonstrates the effectiveness of this control process. Here instead of increasing the gap distance in the switches we changed the breakdown characteristics of the spark gap switches by increasing the gas pressure from 1.15 bar to 1.25 bar leading to an increase of the ignition delay. The figure shows the trigger delay, that is, the time between the signal to the trigger generator and the breakdown of the first spark gap, the delay to ignite the remaining spark gaps of the Marx generator (delay Marx generator), the total delay time as the sum of both curves, and the charging voltage per stage. Initially, the pressure had been stabilized to a trigger delay of 0.4 μs in the first gap for a charging voltage of 35 kV per stage. Raising the pressure to 1.25 bar the delay doubled and became 0.8 μs. It came back to the initial value after the charging voltage was increased to 40 kV.

Since the trigger delay is a statistical process the signals need to be averaged over several shots before an adjustment of the switch gap is made. Naturally the fine tuning of the switch will become easier if the jitter of the trigger delay is small. A small jitter is also required to obtain a good synchronization of several Marx generators. A necessary condition for small jitter is a fast rising trigger pulse. In addition pre-ionization of the spark gap can appreciably reduce this jitter.

For that purpose a passive corona discharge has been applied. The corona discharge is established around a thin wire which is electrically connected to the negatively charged electrode of the spark gap. Because of the electron emission a negative glow discharge is more stable than a positive one. The wire is bent to a ring and mounted at some distance around the electrode gap in such a way, that

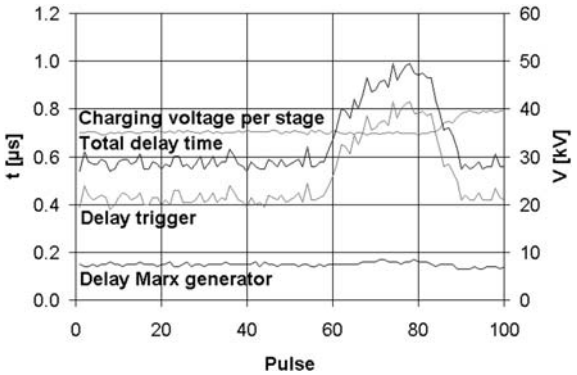

Fig. 7 Demonstration of switch control by measurement of the delay of spark ignition in the first gap. Before pulse 60 the pressure and the charging voltage had been adjusted to 1.15 bar and 35 kV respectively. From pulse 60 on the pressure was gradually raised to 1.25 bar, while the charging voltage was still kept at 35 kV. From pulse 85 on the voltage was readjusted to reach the previous trigger delay of 0.4 µs

the glow discharge around the wire radiates UV light into the gap and onto the electrodes. The ring-like structure causes a symmetric radiation and electron injection fostering together with a homogeneous field distribution a homogeneous wear along the electrode surface. The diameter of the wire and the distance from the electrodes is chosen such that on the one hand the inhomogeneous field around the wire is sufficient to establish the glow discharge. On the other hand, the field inside the space between the wire and the electrodes is chosen low enough to inhibit a direct discharge between the wire and the positive electrode. Figure. 8 shows the equipotential lines of a non optimized configuration with spherical electrodes.

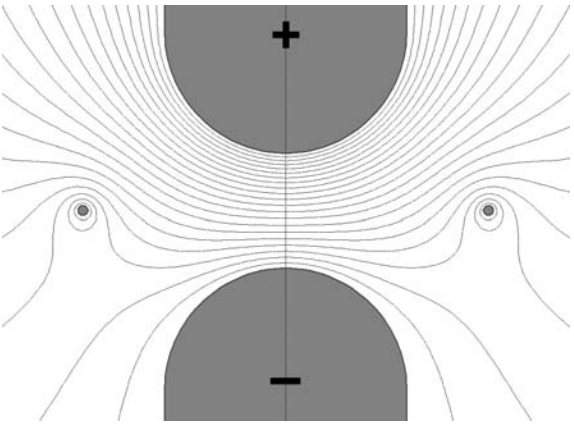

Fig. 8 Equipotential distribution in a spark gap with spherical electrodes surrounded by a corona wire to supply sufficient start electrons before the application of the trigger pulse

To achieve a homogeneous field distribution similar to the field configuration of the undisturbed Borda profile the shape of the electrodes needs further optimization to compensate for to the influence of the corona ring.

It has been experimentally confirmed that a small jitter of the time delay can be achieved with this setup. A jitter ($2\ \sigma$) of the total switching time of less than 92 ns has been obtained for a charging voltage of 90% of the self-breakdown value.

2.5 Screening of the Degree of Electroporation

To verify that the desired degree of electroporation of the treated plant cell tissue is achieved a continuous measurement is required. In principle it is possible to draw samples from the stream of treated plant cells and to determine the achievable product yield in a laboratory. However this procedure seems rather slow and probably not acceptable. Therefore, an in situ measurement technique is necessary.

Such a technique can be based on considerations about the equivalent electric circuit of cell tissue. A single biological cell in a conducting suspension connected to a pulse generator can be represented by the circuitry shown in Fig. 9.

A cell tissue can be modeled by a complex parallel and series arrangement of such equivalent circuits, bridged by additional resistors representing ohmic current paths around the cells, formed, for example, by capillaries (Fig. 10 centre). However, such a network can be formally restructured to a network of the same simplified structure as for a single cell but with values for the elements that depend on the geometry (Fig. 10 right).

The specific resistance of a cell membrane has been measured by Greenham to be of the order of 3000 Ohm cm^2 (Greenham 1966). Pores forming in the membrane cause a reduction of the membrane resistance while the membrane capacitance is little affected. Nevertheless the frequency response of the tissue network can change appreciably.

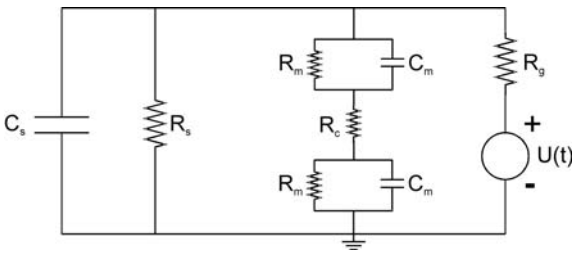

Fig. 9 Equivalent circuit of a biological cell. R_m = membrane resistance, C_m = membrane capacitance, R_c = resistance of cytoplasm, R_s = resistance of suspension outside the cell, C_s = stray capacitance bypassing the cell, R_g = generator impedance, $U(t)$ = time-dependent voltage pulse

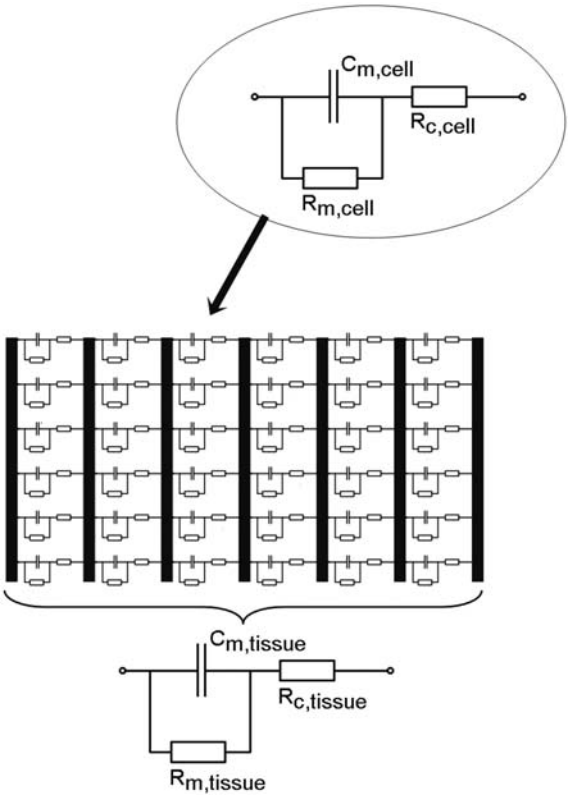

Fig. 10 Simplified equivalent circuits of a single biological cell (*top*) and of cell tissue (*bottom*)

Therefore, it has been proposed to derive the value of $R_{m,tissue}$ from an impedance measurement at two frequencies sufficiently apart and to use the result as a measure of the degree of electroporation that has been achieved (Angersbach et al. 1997, 1999; Lebovka et al. 2000, 2001). At a low frequency in the range of several hundred hertz, the capacitive part of the current through the cell membrane becomes negligible; hence, the sum of $R_{s,tissue}$ and $R_{m,tissue}$ is obtained. At a high frequency in the range of several megahertz, the capacitance is short-circuited and only the value of $R_{s,tissue}$ will be measured. $R_{m,tissue}$ can be calculated from the difference of both results. The cell tissue is considered to be electroporated completely, when $R_{m,tissue}$ has fallen to several ohms. Then the membranes of many cells will have been denatured and the cytoplasm will penetrate into the space outside the cell enclosure. This diffusion process is supported by the inner pressure of the cells.

The described method works fine for small reactors, where the inductivities of the leads can be neglected. Figure. 11 shows the complex impedance of a cubical sugar beet sample in the frequency range between 100 Hz and 10 MHz. It is evident that in this case the upper frequency needs to exceed 5 MHz. To use this method in a large-scale industrial reactor, electrode separations of several 10 cm have to be

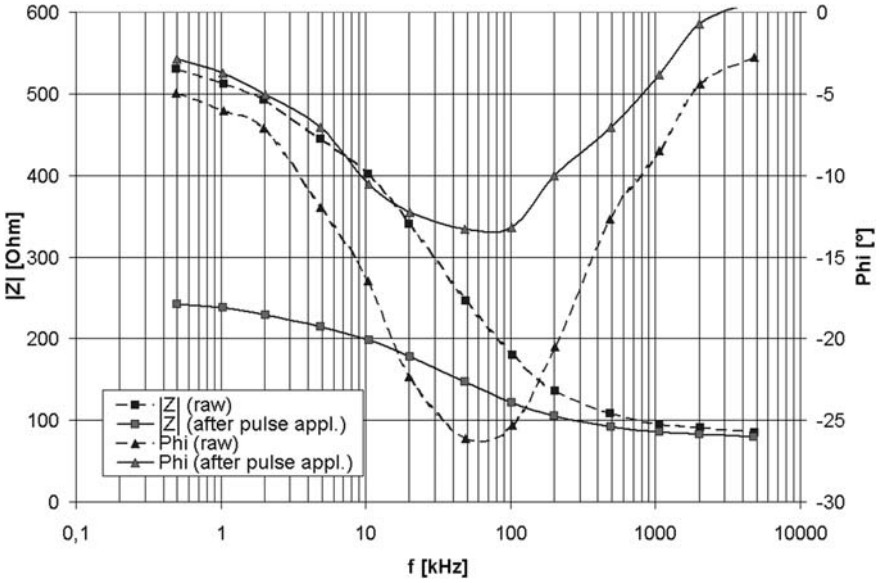

Fig. 11 Complex impedance of a cubical sample (125 cm^3) from a sugar beet both for raw and treated material

bridged. In these cases, one cannot neglect the effect of inductances which together with stray capacitances can form a resonant circuit.

Furthermore, it will take between 1 and 2 s to probe the reactor with two frequencies. Therefore, in a stream of plant material the probed samples will not be identical resulting in erroneous measurements, if the flow is inhomogeneous. A simultaneous measurement at two frequencies could avoid this problem. However in this case it would become necessary to investigate, whether the biological system is linear enough for the two measurement frequencies not to influence each other. Anyway, the measurement device would be more complex.

To overcome these difficulties a new measurement method has been proposed (Sack and Bluhm 2007). It is based on the change of the phase angle between voltage across the sample and current through the sample with frequency. Especially at medium frequencies the influence of the capacitive current flow through the cell membranes on the phase shift becomes quite strong. For sugar beets the phase shift is maximal at approximately 50 kHz, both for raw and partly electroporated beets. As the capacity C becomes more and more shorted while the electroporation progresses, the phase angle decreases and can be taken as a measure for the degree of electroporation that has been reached. If all cells were completely opened, the phase angle should come close to 0° in the ideal case.

Conducting the measurements at frequencies around 50 kHz ensures that the influence of stray inductances remains small. In addition using just a single frequency makes continuous monitoring of the degree of dissociation of the plant cell material

much easier. We can determine the phase shift between the current and voltage signals just from the time difference between their zero crossings.

3 Emerging Industrial Applications

3.1 Treatment of Sugar Beets

Probably the most advanced large scale industrial application of electroporation is the treatment of sugar beets. The standard procedure of sugar production from beets consists of carving the fruits into cossettes and subsequently extracting the juice from these cossettes at elevated temperatures with as little water as possible (Schiweck and Clarke 2001). The sugar dissolved in the cell juice can leave the beet cossettes only if the cell and vacuole membranes have been destroyed. In modern sugar plants this is achieved by thermal denaturation at temperatures above 70°C (Fig. 12). The transport of sugar and other water-soluble substances from the inside of the cossettes to the extraction water occurs by diffusion. Since the diffusion coefficient is temperature dependent the extraction temperature should be as high as possible. However, at too large temperatures, considerable amounts of structural substances from the cell walls are also denatured and become water soluble. Thus impure raw juices are achieved which need extensive processing. Therefore a temperature course is applied which represents a compromise: Denaturation is achieved by heating the cossettes to 70–78°C for a short time and extraction is carried out at 69–73°C.

The temperature course also influences the surviving of microorganisms introduced into the process by soil from the beets. The metabolism of these bacteria can lead to sugar losses. Some organisms are not at all inhibited at the applied temperatures and therefore disinfectants (e.g., hydrogen peroxide and formalin) are generally introduced into the extraction system.

Appreciable energy savings and less expensive purification procedures are conceivable if the juice extraction could be carried out at much reduced temperatures. The use of PEFs as a nonthermal method for the breakage of cell membranes in vegetables has first been described by Doevensbeck and Flaumenbaum (Doevenspeck 1962; Flaumenbaum 1967). Recently it has been proposed to use a combination of pressing and PEF-treatment for the extraction of juice from sugar beets (Bouzrara and Vorobiev 2000, 2001; Jemai and Vorobiev 2003; Eshtiaghi and Knorr 2002). Although this process can lead to a much reduced energy consumption it represents a completely new technology and requires a redesign of the entire sugar plant. Also it seems difficult to scale-up their proposal from the laboratory level to the large throughputs of up to 15 000 t/day required for an economic sugar factory.

Here we restrict the discussion to a different approach which aims at integrating the pulsed electric field treatment into the production line of existing sugar plants as indicated in Fig. 12 (Schultheiss et al. 2002, 2004).

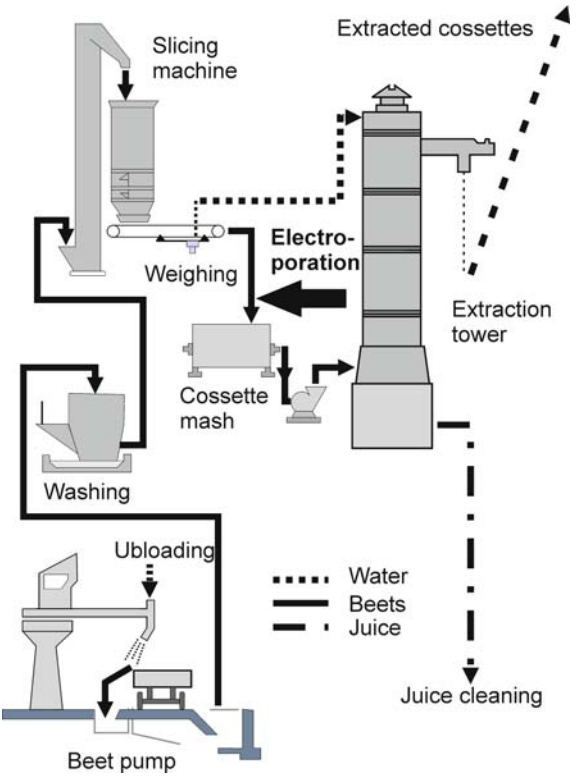

Fig. 12 Entrance stage of a conventional sugar factory

To demonstrate the potential advantages of electroporation for the extraction of juice from sugar beet cells the mobile test device KEA (**K**arlsruher **E**lektroporations **A**nlage – Karlsruhe electroporation device) was built in the Research Centre Karlsruhe and used in several experimental campaigns at a sugar factory. A general view of the facility is shown in the left part of Fig. 13. The treatment chamber shown in the right part was built from a polypropylene-tube of 18 cm inner diameter. It contains four electrode pairs constructed from stainless steel. Each pair consisted of two disk shaped electrodes of 4 cm diameter, axially and azimuthally displaced by 16 cm and 90° respectively. The twisted electrode pairs secured that each cell of an entire sugar beet passing through the tube had seen at least the minimum field at the centre between two electrodes. At nominal pulse voltage this field reached a value of in average 8.8 kV/cm. The treated beets leaving the reaction tube were transported to a tub with the help of a screw conveyor visible on the left side in Fig. 13. A maximum throughput of 300 kg/hour could be handled with this setup.

High voltage pulses with amplitudes of up to 220 kV were created with the help of a six-stage low-impedance Marx generator. Discharging the Marx into the reaction chamber a unipolar pulse of about 1 μs duration is achieved. Each pulse

Fig. 13 The mobile test device KEA used to demonstrate the potential advantages of electroporation for the production of sugar from sugar beets. The left part shows the complete set up. The photo on the right depicts the treatment vessel

represents an electrical energy of 0.75 kJ. The Marx was capable to run at a repetition rate of 10 Hz. Both the Marx generator and the reaction tube were housed in a Faraday cage to eliminate the emission of electromagnetic noise. The high voltage supply is a 10 kW commercially available unit.

At first entire sugar beats were treated. After treatment they were cut into pieces and either cold pressed or extracted in water at different temperature levels. Figure 14 shows a cut through sugar beets before and after treatment in the reaction chamber together with the corresponding yield of juice obtained by cold pressing with 32 bar pressure for 15 min. Juice droplets appearing on the cut surface of the treated beet are indicative that the cell membranes have been destroyed by the

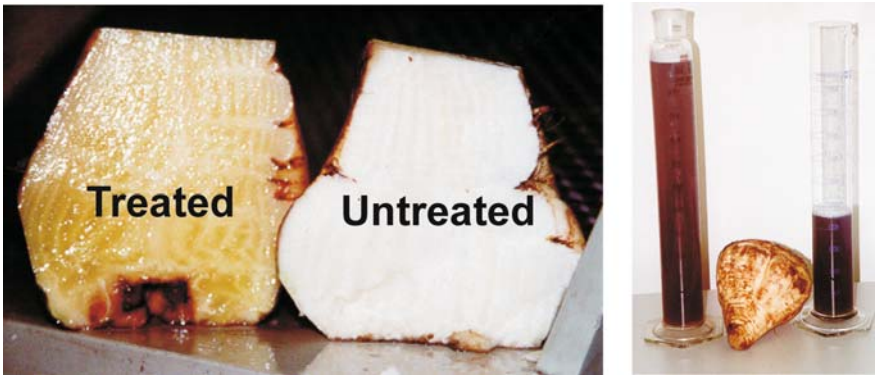

Fig. 14 Cut through sugar beets before and after treatment in the reaction chamber together with the corresponding yield of juice obtained by cold pressing with 32 bar pressure for 15 minutes

pulsed electric fields. It has been found that the same specific yield as through thermal denaturation at 72°C could be achieved with much lower specific energy input. Thus, it is evident that electric pulse treatment has a large potential for energy saving.

Besides by cold-pressing the sugar beets treated in the KEA reaction chamber were also extracted by diffusion into water. It was found that the same sucrose extraction as in the standard procedure at 72°C could be achieved at lower temperatures. Since the mobility of the sugar molecules decreases with falling temperature longer extraction times would become necessary at too low temperatures, thus reducing the achievable mass throughput. Therefore, a compromise has to be found, which is considered to be below 70°C. At this temperature a thermal dissociation of cell substances does not yet occur and we can expect a purer raw juice draft.

As shown in Fig. 15 this has indeed been observed. Here the raw juice purity—defined as the sucrose fraction in the juice—has been plotted versus the cossette purity—defined as the ratio of sugar to the total solid mass in the beet. It is seen that especially for beets of lower quality electroporation and extraction at lower temperatures lead to improved juice purity. Generally there is always a mixture of beet qualities entering the sugar factory.

In addition to the benefits described above it has also been found that the raw juice draft (i.e., weight of juice/weight of beet), which in the standard procedure is around 110%, could be significantly reduced, without changing the sucrose extraction. For thermal reasons it is desirable to attain the lowest possible raw juice draft.

Summarising the results, it is obvious that replacing the normal thermal treatment at elevated temperatures (>70°C) for denaturation by the application of pulsed electric fields in the process line of a sugar factory leads to numerous advantages. There are two major areas for energy saving in a sugar factory by adding an electroporation step to the process line: Extraction can be carried out at lower temperatures and with

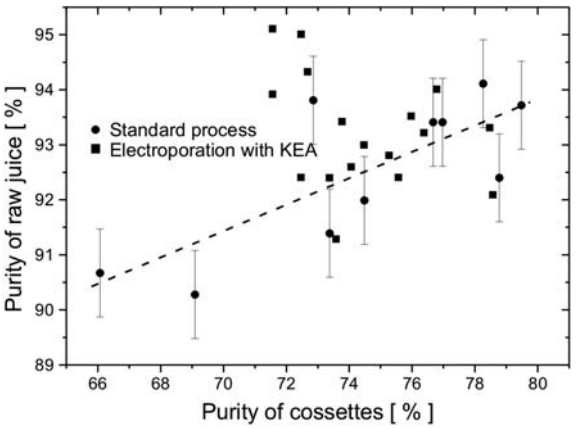

Fig. 15 Raw juice purity versus cossette purity. At low beet quality the raw juice purity obtained from treatment with PEFs is superior

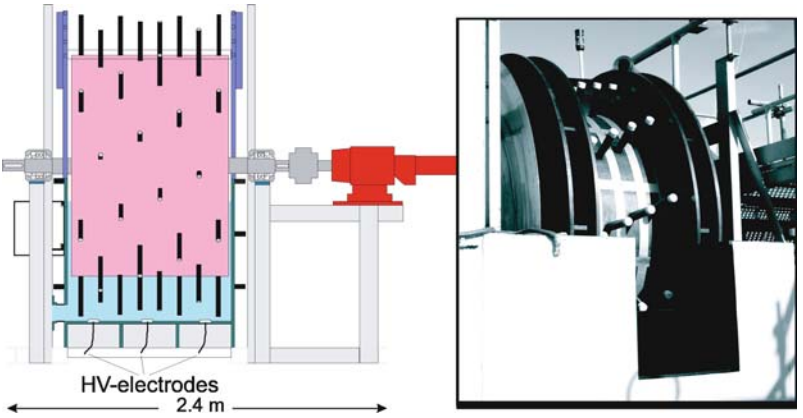

Fig. 16 Transport drum and reactor vessel of the 10 t/hour sugar beet electroporation facility KEA-ZAR

lower raw juice draft. It seems feasible to integrate the electroporation step into the process line without requiring major changes of the other components of the sugar plant.

Encouraged by the findings with the mobile plant the demonstration plant KEA-ZAR was built at a factory site (Frenzel et al. 2005). This facility allowed a throughput of up to 10 t/hour. Its reaction chamber consisted of a coaxial cylindrical set up. The inner cylinder providing the beet transport was a plastic drum with spikes protruding from its surface (Fig. 16). The high-voltage electrodes were placed in the jacket of the outer cylinder. The ground electrodes were stainless steel ribbons mounted on the jacket of the inner cylinder.

The pulses were supplied from the two seven-stage Marx generators shown in Fig. 3, each delivering pulses with an amplitude of 210 kV at a frequency of 20 Hz. The complete facility is shown in Fig. 17. KEA-ZAR could demonstrate that the advantages of electroporation for the extraction of sugar from sugar beets can also be realized under the conditions of industrial production and the operating experience gained with KEA-ZAR will enter into the design of the next demonstration plant fully integrated into the factory and designed to treat a partial stream of up to 1500 t/day. KEA-ZAR has also shown that field homogeneity is important for the complete destruction of all beet cells.

Another important parameter for the disintegration of beet cells is the temperature at which the treatment is carried out. This is shown in Fig. 18, where the yield of juice has been plotted as a function of temperature for equal pulse parameters (30 pulses with $E = 3$ kV/cm). Since beets are harvested in autumn and stored outside, their temperature can become close to 0°C. Experiments showed, that the amount of electrical energy needed for complete denaturation of cells increases with decreasing temperature (Frenzel et al. 2005). Therefore, an optimum processing strategy has to be developed, that is, comparing the costs for the delivery of higher electric fields with those of preheating the beets using the waste heat from the

Fig. 17 Prototype facility KEA-ZAR during construction at the factory site

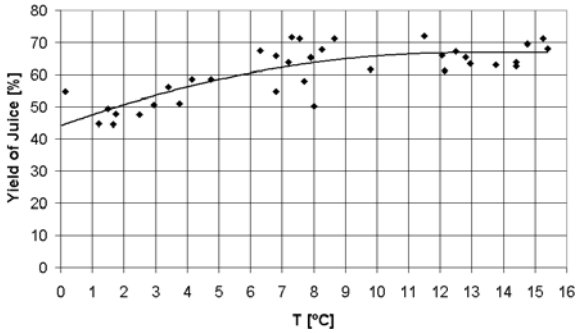

Fig. 18 Yield of juice from sugar beet samples as a function of temperature for equal pulse protocols (30 pulses of 3 kV/cm)

concentration of raw juice in the later process stages of the factory. However, to warm up the entire stream of beets in the sugar factory seems not feasible because of the rather large thermal time constants. Therefore, it is more advantageous to cut the beets into cossettes which because of their smallness need much shorter times to warm up before treatment. An additional advantage of cossettes is that they allow a simpler transport concept without mechanical elements.

3.2 Treatment of Grapes

Bouquet, taste, and color of wine are decisively determined by the degree of disintegration of the skin cells of wine berries. Commonly this is either achieved by mash fermentation or by mash heating. In the first case alcohol is produced which then acts as the extractive agent (aqueous-alcoholic extraction). The disadvantage

of this process is that it is time consuming and therefore expensive. Mash heating (aqueous-thermal extraction) is quicker and very often supported by the addition of enzymes.

Electroporation of wine grapes is an alternative non-thermal process completed in a few seconds leading to a prudent extraction of colors and valuable constituents within hours (Eshtiaghi and Knorr 2000; Tedjo et al. 2002).

To explore the capabilities of electroporation for the production of wine a facility allowing a throughput of several tons per hour is required. Thus, it is possible to look into the complete process chain up to the final product. For that purpose the specially designed mobile facility KEA-Wein, shown in Fig. 19, has been built at the Research Centre Karlsruhe and operated in several campaigns between 2001 and 2006 together with the State-Institute on Wine-Cultivation in Freiburg, Germany and the company KEA-TEC GmbH (Sigler et al. 2005). KEA-Wein, was able to produce electric fields of up to 60 kV/cm in the reactor at a repetition rate of up to 15 Hz. It was able to handle a throughput of up to 1 t/hour at a connected wattage of 15 kW. The average specific energy consumption was around 15 kW-hour/t. To prevent a flash-over inside the reactor due to air bubbles the must can be pressurized up to a pressure of 8 bar.

Both red and white wine grapes have been treated (Sigler et al. 2005). Red Burgundy mash has first been electroporated in 2001 and compared to a control sample that was disintegrated by the usual heating process. To extract color and tanning substances both samples were left to stand for one night and then pressed, precleared and fermented into wine. As shown in Table 4 the tanning and acid concentrations of the electroporated must samples were somewhat lower than those of the control samples. However this can probably be changed by varying the electrical parameters. Nevertheless, the basic analytic data of the finished wine, especially the color and tanning agent values came very close to those of the control specimen.

Fig. 19 Mobile facility KEA-Wein for the treatment of grape mash with strong PEFs

Table 4 Basic analytic data for red burgundy must and wine (2001) (Sigler et al. 2005)

	Must (precleared)				Wine									
	Must sweetness (°Oe})	Centrifugal sludge (%)	Tanning substances (g/l)	Total acid (g/l)	Alcohol (g/l)	Total Extract (g/l)	s.fr.. Extract (g/l)	Total acid (g/l)	Free SO_2 (mg/l)	Total SO_2 (mg/l)	Tanning substances (g/l)	Color intensity	Color shade	Quality f. [1] (n = 48)
Control (MH)	96.5	1.21	2.8	8.3	98.5	25.1	23.8	4.7	48	131	2.1	2.47	0.95	2.17
Electro-poration	96.0	1.37	2.3	6.9	104	24.7	23.2	4.1	51	121	2.0	2.33	1.02	2.15

Blind tasting by 48 knowledgeable persons resulted in indistinguishable quality ranking between both wines.

Additional campaigns were carried out in 2003 and 2004. It was the aim to reduce the centrifugal sludge content further by optimizing the hydraulic transport through the reactor and to extend the treatment to other types of grapes. The results were similar as in 2001 and showed especially high contents of digestible nitrogen in the must. Always rather high field strengths, on the order of 50 kV/cm, were required to get satisfactory color extraction. This finding has been attributed to the smallness of vacuoles in the cells of the skins containing the color (Fig. 20). Also it became apparent that the nonthermal aqueous extraction conditions allow new modified red

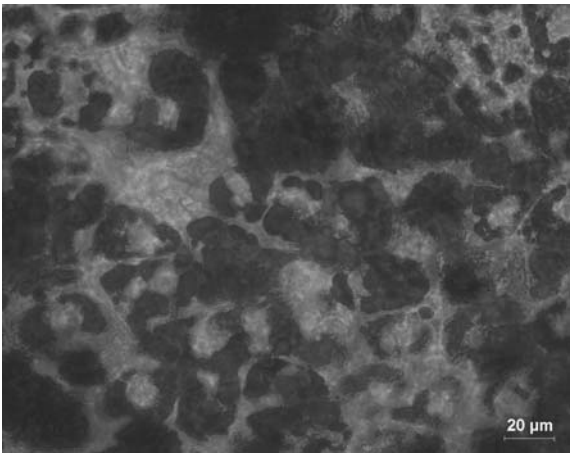

Fig. 20 Microscopic picture of peel tissue of red Burgundy wine grapes showing several small, irregularly shaped color containing vacuoles per cell

wine profiles. Future experiments shall exploit this potential and evaluate whether a combination between electroporation and fermentation can lead to advantages.

From the vintage in 2002 Riesling mash without stalks has been treated. Both, the control and the electroporated sample were pumped through the facility. Therefore, the mechanical stress was equal and any differences in the result could solely be attributed to the effect of electroporation. For further comparison mash has also been prepared by whole-berry pressing (WBP). The results are presented in Table 5. As expected the must from the latter treatment showed the lowest sludge content while the electroporated sample had the highest sludge fraction. However in the precleared must the differences became small. Strikingly the must obtained from the electroporated mash showed lower acid values but higher contents of tanning agents and yeast digestible nitrogen. The finished wine from the electroporated variant was still characterized by a larger content of tanning substances and a larger amount of sugar free extract. Also remarkable is the higher fraction of potassium indicating complete cell disintegration.

Of much interest in the field of white wine preparation is the liberation of aromas and their precursors especially from the peels of the berries. Electroporation clearly led to the largest amount of aromas in the wine.

A sensual examination of the finished wines by 50 butlers clearly put the electroporated wine in the first rank and graded its quality with the highest valuation. In 2005 these results were confirmed for bouquet wines like Traminer.

Thus in the domain of white wines electroporation improves the extraction of type specific aromas and aroma precursors. As shown in Fig. 21 electroporation produces the highest yield of terpenes and other aroma substances.

Summarizing, electroporation of grapes allows an effective and prudent extraction especially of those substances contained in the cells of the berry skin. Therefore,

Table 5 Basic analytic data for Riesling must and wine (2002) (Sigler et al. 2005)

	Must (precleared)				Wine									
	Must sweetness (°Oe)	Centrifugal sludge (%)	Tanning substances (g/l)	Total acid (g/l)	Dig. Nitrogen	Alcohol (g/l)	Total Extract (g/l)	s.fr.. Extract (g/l)	Total acid (g/l)	Free SO_2(mg/l)	Total SO_2(mg/l)	Tanning substances (g/l)	Potassium (g/l)	Ranking. (n = 50)
WBP Comparison	82	0.80	0.22	11.1	25	99.0	21.5	18.2	6.7	44	85	0.26	498	2.3
Control (pumped)	77	0.97	0.33	9.2	32	96.2	19.4	19.3	6.7	43	83	0.33	585	2.5
Electroporation	79	0.80	0.57	8.6	37	98.9	20.6	20.5	6.8	41	92	0.38	776	1.3

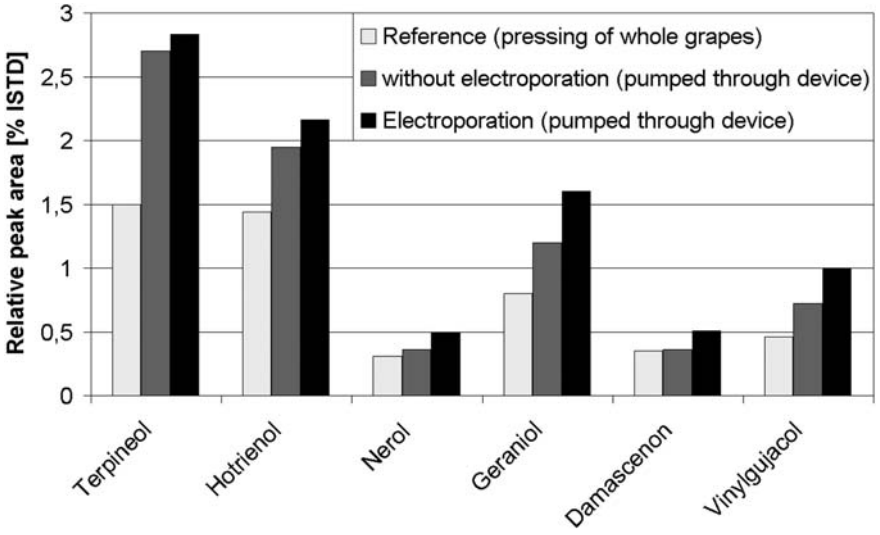

Fig. 21 Aroma substances in Riesling wine after different kinds of processing

it offers the potential to develop wines of new characters and flavors. It can either be applied as a self-contained method or in combination with common methods. In case of red must preparation it can lead to economic advantages by either reducing the energy cost or the time for color extraction. Despite these obvious advantages a license for the use of electroporation in wine production is still pending.

3.3 Conditioning of Green Biomass by Electroporation Assisted Dewatering

To exploit the unrealized energetic capacity of biomass, which has been estimated to potentially cover up to 20% of the present energy consumption in Europe, it is indispensable to cultivate energy plants.

Among all sources, agriculture has the largest potential for a directed production of energetically useable biomass. Therefore it is to be expected that the cultivated area for energy plants like corn, lupines, etc., shall grow appreciably. In addition new cultivation concepts like the two-culture utilization system promise an essential increase in the yield of dry biomass while simultaneously relieving cultivated ecosystems (Scheffer 2003). In this concept it is intended to harvest nonripened plants. However, their energetic utilization requires new concepts for preservation and dewatering. Commonly ensilage is presently used for preservation. But the energetic utilization of silage especially for the production of liquid fuel from biomass (biomass to liquid (BTL) process) requires extensive dehydration by pressing and heating.

As depicted in Fig. 22 electroporation could support drying and establish a new procedure for preservation of green biomass. It is conceivable that the degradation

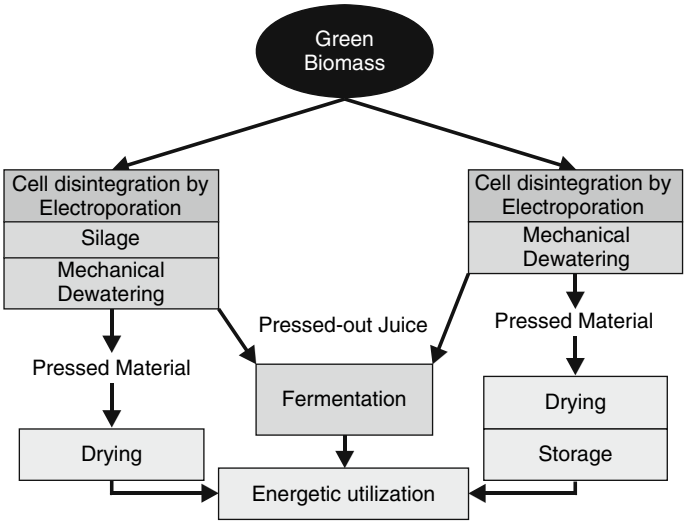

Fig. 22 Concept of electroporation assisted dewatering of green biomass. The figure shows the two possible paths to store biomass and to prepare it for utilization in a BTL process

of cells before ensilage facilitates the pressing of silage. An alternative preservation concept, which becomes especially attractive for the green biomass produced in the two-culture concept, can be based on electroporation assisted pressing and additional drying by heating. If the degree of moisture in the dried biomass falls below 15–20%, it becomes storable for longer time.

The pressed-out juice contains fine grinded and easily solvable and breakable organic substances and is therefore considered as the ideal substrate for further utilization in biogas plants.

For the electroporation of plant material, a good electric contact to the electrodes is essential. Therefore, usually the material is either suspended in water or treated as mash. But for the dewatering of green biomass aiming at rather low water contents both methods cannot be applied. Any process water added for electroporation has to be removed in the subsequent drying step.

Hence, some water from the plant material is extracted in a pressing step before electroporation. The juice fills the space between the plant material and the electrodes and displaces the air. Moreover, this step compacts the material and thus improves the effectiveness. During electroporation the mechanical pressure is kept constant. The electroporation-assisted dewatering process starts already during pulse application. In case of a batch process with the force applied through a piston, the piston moves down a bit as the water is extracted from the opened cells.

After electroporation water is further extracted by pressing. As an example Fig. 23 shows the relative contents of dry mass and juice with water soluble substances for young maize plants after electroporation and the subsequent pressing step after varying numbers of pulses at a field strength $\hat{E} = 7$ kV/cm and a pulse

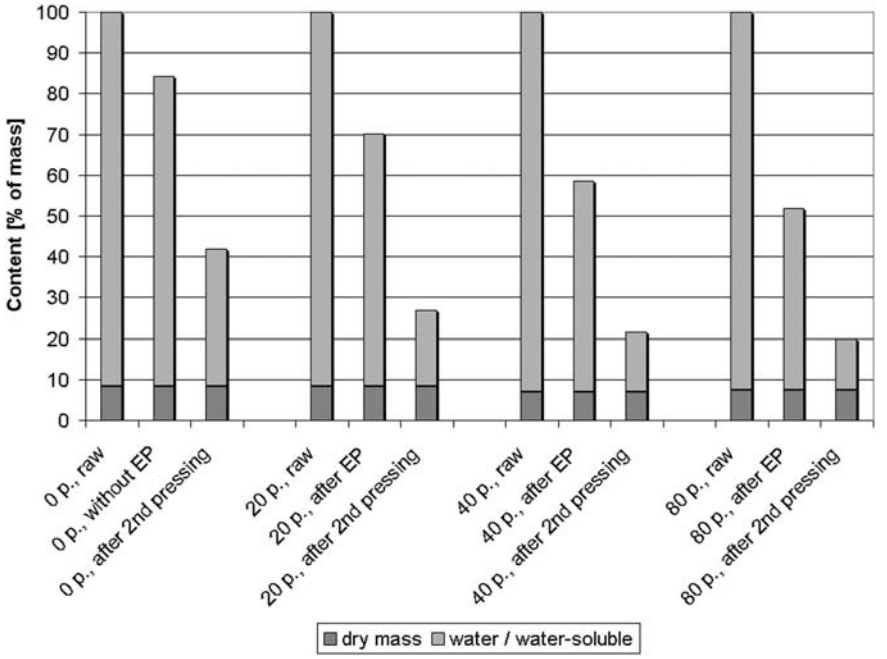

Fig. 23 Relative contents of dry mass and water with water-soluble substances for young maize plants after electroporation with growing numbers of pulses ($\hat{E} = 7$ kV/cm, $t_h = 1.6$ µs) and a subsequent pressing step (Sack et al. 2007)

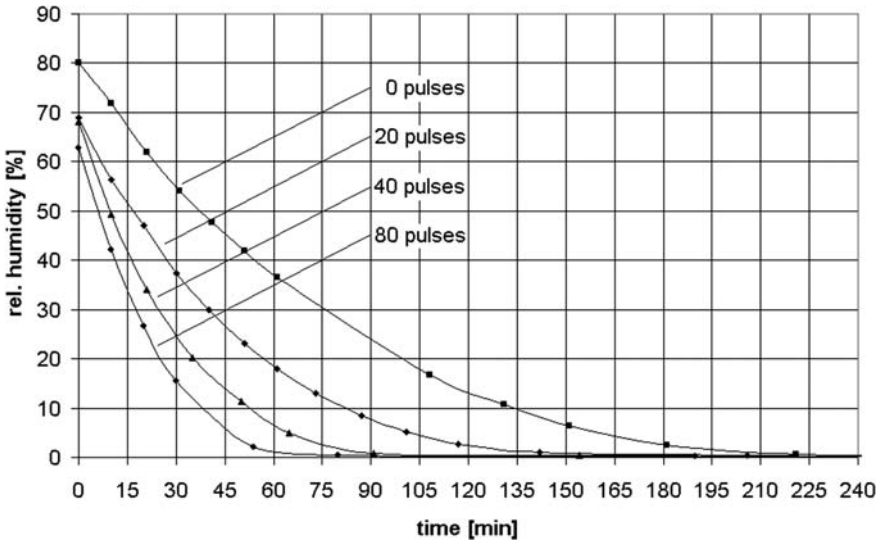

Fig. 24 Temporal decrease of the relative humidity for young maize plants during thermal drying at 105°C ($\hat{E} = 7$ kV/cm, $t_h = 1.6$ µs). The curves are for plants treated with different numbers of pulses

duration of $t_h = 1.6$ μs. Without electroporation approximately 63% of the juice can be extracted. This fraction increases with the number of applied pulses to 85% after applying 80 pulses. Nevertheless the relative humidity in this case is still 63%.

The required relative humidity of 15–20% is achieved in a subsequent drying process. Fig. 24 shows the temporal decrease of the relative humidity during a thermal drying process in an oven at 105°C. The electroporation-assisted drying enables a much faster processing. The diagram shows that after application of 80 pulses the threshold value of 20% relative humidity is reached in one quarter of the time needed for nonelectroporated material.

In Fig. 25 the required energy per kg of dry mass to achieve a relative rest humidity of 0% and 20% for young maize plants treated with different numbers of electrical field pulses has been plotted. Here the energies were divided into energy for electroporation and energy for evaporation. The electric energy required for electroporation was always small compared to the thermal energy for the drying process. In case of 80 pulses it amounted to 150 kJ per kilogram dry mass while the necessary thermal energy became about 3700 kJ/kg. Without electroporation a total specific energy of approximately 10000 kJ/ kg was needed. These findings clearly demonstrate a considerable energy saving potential. However, a complete

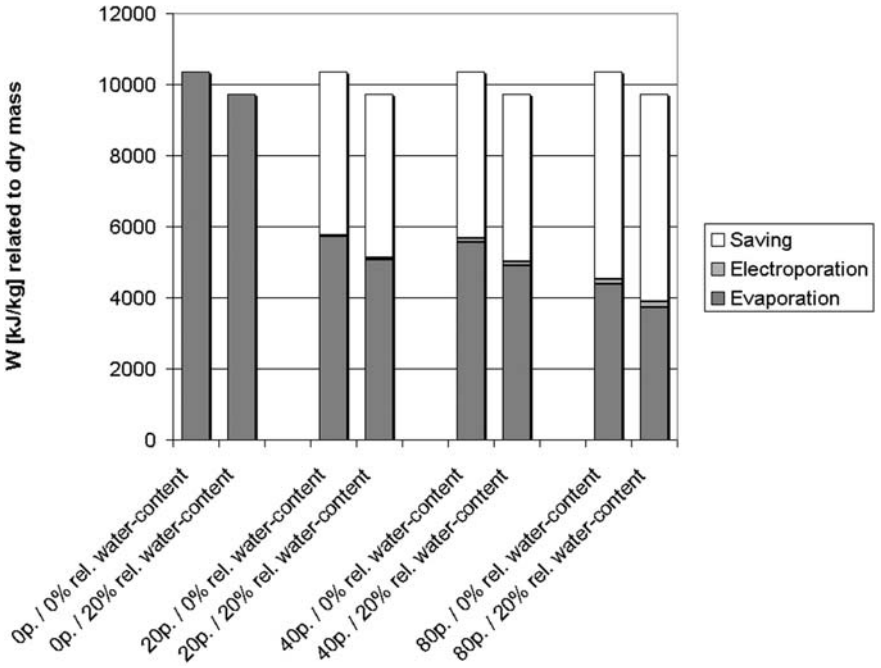

Fig. 25 Required energy per kg of dry mass to achieve relative rest humidity of 0% and 20% respectively for young maize plants treated with different pulse numbers ($\hat{E} = 7$ kV/cm, $t_h = 1.6$ μs). The energies have been split into energy for electroporation and evaporation

energy balance still needs a more careful consideration of heat recycling and to take into account the efficiency of electric energy conversion in the electroporation step.

References

Angersbach A, Heinz V, Knorr D (1997) Elektrische Leitfähigkeit als Maß des Zellaufschlussgrades von zellulären Materialen durch Verarbeitungsprozesse. LVT 42(4): 195–200.

Angersbach A, Heinz V, Knorr D (1999) Electrophysiological model of intact and processed plant tissues: cell disintegration criteria. Biotechnol. Programm. 15: 753–762.

Belkin GS (1971) Dependence of electrode erosion on heat flux and duration of current flow. Sov. Phys. Tech. Phys. 15(7): 1167–1170.

Belkin GS and Kiselev VYa (1977) Effect of the medium on the electrical erosion of electrodes at high currents. Sov. Phys. Tech. Phys. 23(1): 24–27.

Bluhm H (2006) Pulsed Power Systems. Springer, Berlin, Heidelberg, New York.

Borda JC (1766) Sur l'écoulement des fluids par les orifices des vases. Mém. Acad. Roy. Sciences, Année 1766: 579–607.

Bouzrara H, Vorobiev E (2000) Beet juice extraction by pressing and pulsed electric fields. Int. Sugar J. 102(1216): 194–200.

Bouzrara H, Vorobiev E (2001) Nicht-thermisches Pressen und Auswaschen von frischen Zuckerrübenschnitzeln kombiniert mit der Anwendung eines pulsierenden elektrischen Feldes. Zuckerindustrie 126: 463–466.

Doevenspeck H (1962) Über die Beeinflussung von Zellen und Zellverbänden durch elektrostatische Impulse. Archiv für Lebensmittelhygiene 13(3): 68–69.

Donaldson AL (1990) Lifetime considerations. In: Gas discharge closing switches. G. Schaefer, M. Christiansen, and A. Guenther Eds., Plenum Press, New York: 325–344.

Donaldson AL (1991) Electrode erosion in high-current, high-energy transient arcs. Thesis Texas Tech University, Lubbock, Texas USA.

Eshtiaghi M, Knorr D (2000) Anwendung elektrischer Hochspannungsimpulse zum Zellaufschluss bei der Saftgewinnung am Beispiel von Weintrauben. LVT 45(1): 23–27.

Eshtiaghi M, Knorr D (2002) High electric field pulse pretreatment: potential for sugar beet processing. J. Food Eng. 52: 265–272.

Flaumenbaum B (1967) Anwendung der Elektroplasmolyse bei der Herstellung von Fruchtsäften. Die Lebensmittel-Industrie 8: 19–22.

Frenzel S, Michelberger T, Sack M, Bluhm H, Kern M (2005) Entwicklung und Bau einer Elektroimpuls-Pilotanlage. Abschlussbericht, Förderkennzeichen 0330434, *TIB-Hannover,* 2005.

Greenham CG (1966) The Relative Electrical Resistances of the Plasmalemma and Tonoplast in Higher Plants. Planta (Berl.) 69: 150–157.

Haufe W, Reichel W, Schreiner H (1972) Losses of varying types of CuW sintered impregnation material in the air at high current levels. Zeitschrift für Metallkunde 63(10): 651–654.

Jemai A, Vorobiev E (2003) Enhanced leaching from sugar beet cossettes by pulsed electric fields. J. Food Eng. 59: 405–412.

Kind D (1958) Die Aufbaufläche bei Stoßspannungsbeanspruchung technischer Elektrodenanordnungen in Luft. Elektrotechnische Zeitschrift 79(3): 65–69.

Lebovka N, Bazhal M, Vorobiev E (2000) Simulation and experimental investigation of food material breakage using pulsed electric field treatment. *J.* Food Eng. 44: 213–223.

Lebovka N, Bazhal M, Vorobiev E (2001) Pulsed electric field breakage of cellular tissues: Visualisation of percolative properties. Innov. Food Sci. Emerging Technol. 2: 113–125.

Marx E (1923) Verfahren zur Schlagprüfung von Isolatoren und anderen elektrischen Vorrichtungen. German Patent 455933.

Marx E (1924) Versuche über die Prüfung von Isolatoren mit Spannungsstößen. Elektrotechnische Zeitschrift 25: 652–654.

Sack M, and Bluhm H (2005) Long-term Test of a Triggered Marx Generator, Proc. Pulsed Power Conference 2005, Monterey, DVD-ROM.

Sack M and Bluhm H New Measurement Methods for an Industrial Scale Electroporation Faciltity for Sugar Beets, Proc. OPTIM 2006, Vol. 1 pp. 135–140, Brasov, Romania, May 18–19, 2006.

Sack M, Eing C, Buth L, Berghöfer Th, Frey W, Bluhm H (2007) Electroporation as an optimizing step in the drying of green biomass, Proc. Pulsed Power and Plasma Science Conference, Albuquerque 2007, DVD-ROM.

Sack M, Schultheiss C, Bluhm H (2003) Wear-less Trigger Method for Marx Generators in Repetitive Operation. 14th IEEE Pulsed Power Conf., Dallas, Tex., June 15–18, 2003.

Sack M, Schultheiss C, and Bluhm H (2005) Triggered Marx Generators for the Industrial-Scale Electroporation of Sugar Beets. IEEE Trans. Industry Applications, 41(3): 707–714.

Scheffer K (2003) Der Anbau von Energiepflanzen als Chance einer weitere Ökologisierung der Landnutzung, Mitt. Ges. Pflanzenbauwiss. 14: 114–119.

Schiweck H, Clarke M (2001) In: Ullmann's Encyclopedia of Industrial Chemistry, Sixth Edition, 2001 Electronic Release, Wiley-VCH, Weinheim, Germany.

Schultheiss C, Bluhm H, Mayer H, Kern M, Michelberger T, Witte G (2002) Processing of sugar beets with pulsed electric fields. IEEE Trans. on Plasma Science 30(4): 1547–1551.

Schultheiss C, Bluhm H, Mayer H-G, Sack M, Kern M (2004) Die Wirkungsweise der Elektroporation und die Entwicklung industrieller Anlagen. Zuckerindustrie 129(1): 40–44.

Sigler J, Schultheiss C, Kern M (2005) Maischeporation – ein neuer Weg der Weinbereitung. Schweiz. Z. Obst-Weinbau 16: 14–16.

Tedjo W, Eshtiaghi M, Knorr D (2002) Einsatz nicht-thermischer Verfahren zur Zell-Permeabilisierung von Weintrauben und Gewinnung von Inhaltsstoffen. Flüssiges Obst 9: 578–583.

Tsukamoto S, Maeda T, Ikeda M, and Akiyama H (2003) Application of pulsed power to mushroom culturing. Proc. 14th Pulsed Power Conference, pp. 1116–1119, Dallas 2003.

Zingerman AG (1960) Thermal theory of the electrical erosion of metals. Electrom. 5(1): 1427–1485.